Title	The effect of fluence rate and wavelength on the formation of protoporphyrin IX photoproducts
Author(s)	Ogbonna, Sochi J.; Masuda, Katsuyoshi; Hazama, Hisanao
Citation	Photochemical and Photobiological Sciences. 2024, 23, p. 1627-1639
Version Type	VoR
URL	https://hdl.handle.net/11094/98910
rights	This article is licensed under a Creative Commons Attribution 4.0 International License.
Note	

ORIGINAL PAPERS

The effect of fluence rate and wavelength on the formation of protoporphyrin IX photoproducts

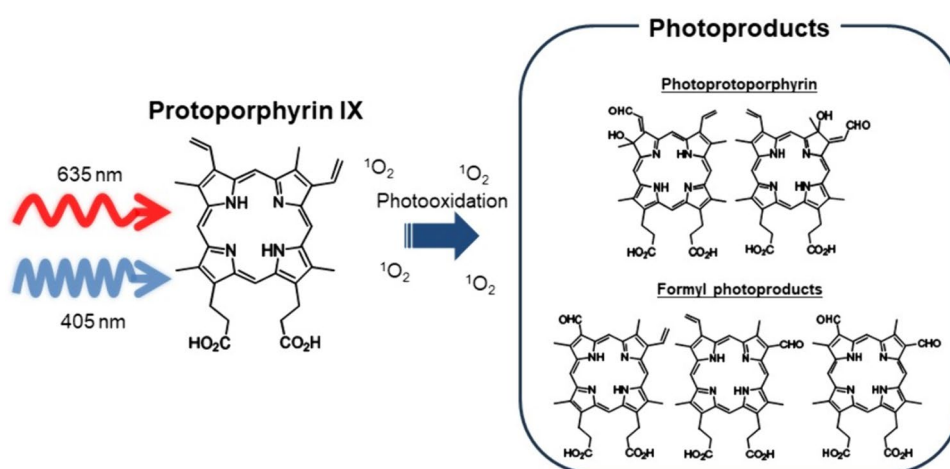Sochi J. Ogbonna[1] · Katsuyoshi Masuda[1,2] · Hisanao Hazama[1]

Abstract

Photodynamic diagnosis and therapy (PDD and PDT) are emerging techniques for diagnosing and treating tumors and malignant diseases. Photoproducts of protoporphyrin IX (PpIX) used in PDD and PDT may be used in the diagnosis and treatment, making a detailed analysis of the photoproduct formation under various treatment and diagnosis conditions important. Spectroscopic and mass spectrometric analysis of photoproduct formation from PpIX dissolved in dimethyl sulfoxide were performed under commonly used irradiation conditions for PDD and PDT, i.e., wavelengths of 405 and 635 nm and fluence rates of 10 and 100 mW/cm^2. Irradiation resulted in the formation of hydroxyaldehyde photoproduct (photoprotoporphyrin; Ppp) and formyl photoproduct (product II; Pp II) existing in different quantities with the irradiation wavelength and fluence rate. Ppp was dominant under 635 nm irradiation of PpIX, with a fluorescence peak at 673 nm and a protonated monoisotopic peak at m/z 595.3. PpIX irradiation with 405 nm yielded more Pp II, with a fluorescence peak at 654 nm. A higher photoproduct formation was observed at a low fluence rate for irradiation with 635 nm, while irradiation with 405 nm indicated a higher photoproduct formation at a higher fluence rate.

The photoproduct formation with the irradiation conditions can be exploited for dosimetry estimation and may be used as an additional photosensitizer to improve the diagnostics and treatment efficacies of PDD and PDT. Differences in environmental conditions of the present study from that of a biological environment may result in a variation in the photoproduct formation rate and may limit their clinical utilization in PDD and PDT. Thus, further investigation of photoproduct formation rates in more complex biological environments, including in vivo, is necessary. However, the results obtained in this study will serve as a basis for understanding reaction processes in such biological environments.

Graphical abstract

Extended author information available on the last page of the article

1 Introduction

Protoporphyrin IX (PpIX), a photosensitizer generated from its precursor 5-aminolevulinic acid (ALA), is commonly used in photodynamic diagnosis (PDD) and therapy (PDT) of tumors and non-malignant diseases [1, 2]. PDD and PDT have high precision and are minimally invasive methods of diagnosis and treatment owing to the photosensitizer's ability to accumulate on cancer cells selectively [3, 4]. Appropriate dose estimation is necessary for improved diagnosis and treatment. However, the direct monitoring of the dosimetry factors, such as the photosensitizer and oxygen concentration, as well as the light fluence to the target area during diagnosis and treatment, can be complex [5]. As an alternative approach, the photosensitizer photobleaching rate can be used as an implicit method of dosimetry, as photobleaching depends on the factors necessary for dosimetry estimation [5–7].

Photoproducts are formed concomitantly with photobleaching when photosensitizers are exposed to light during PDD and PDT. The formation of the PpIX photoproducts has been observed in organic solvents [8–10], cells [2, 5, 6], and in vivo [11, 12]. These photoproducts are formed by the reaction of PpIX with radicals and singlet oxygen when irradiated [13, 14]. Hence, the rate of photoproduct formation could be a complementary approach for monitoring the photosensitizer and oxygen concentration during PDD and PDT [2, 15]. Some PpIX photoproducts are fluorescent and have photosensitizing effects [2, 14, 16–20]. They can potentially be employed as photosensitizers and may enhance diagnostic and treatment efficacy. Investigating the photoproduct formation rate under various treatment and diagnosis conditions would help in their application in PDD and PDT. Some studies have investigated their formation mechanisms and determined their fluorescence emission and absorption bands [2, 5, 6, 11–13]. Unfortunately, a detailed rate of their formation is lacking.

The photochemical reaction resulting in the formation of PpIX photoproducts can vary in solution and in vivo, and their formation may differ based on the environment [2, 8]. Photoproduct formation is affected by factors such as light, oxygen, pH, the concentration of the photosensitizer, and the area of intracellular localization of the photosensitizer [2]. In order to perform a detailed analysis of the photoproduct formation and understand the photochemical reaction leading to photoproduct formation, analysis has to be conducted in a controlled environment. However, manipulating these factors in vivo is difficult [5]. Further, influence on the reaction mechanism and rate may occur due to the presence of different biomolecules, some of which are oxidizable [8]. To understand the photochemical reaction leading to photoproduct formation in a complex biological system, it is necessary to first understand their formation in a simple environment.
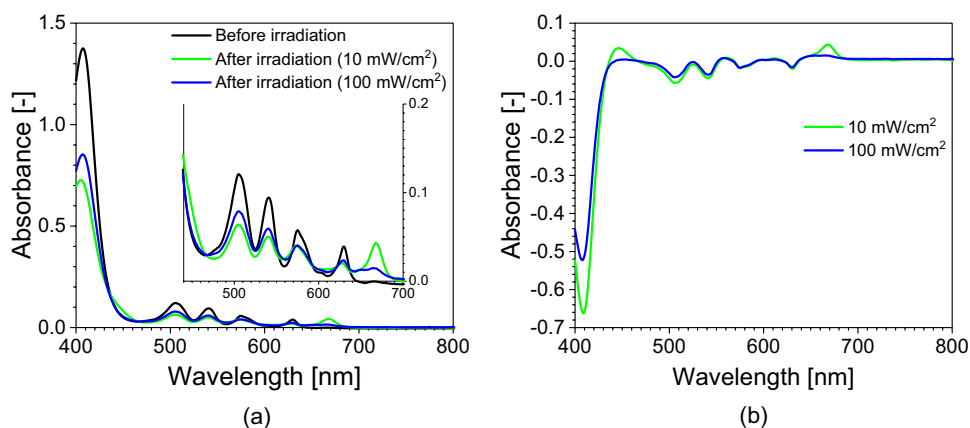
In the present work, an analysis of the formation of photoproducts under exposure to lights at the wavelengths of 405 nm (used in PDD) and 635 nm (used in PDT) has been performed for PpIX in an organic solvent. Dimethyl sulfoxide (DMSO) was employed as the solvent to avoid aggregation due to the highly hydrophobic nature of PpIX [21]. Spectroscopic and mass spectrometric analyses of photoproduct formation under two irradiation wavelengths at two irradiation fluence rates were investigated, and the effect of fluence rate on the photoproducts was studied. The analysis performed in this work serves as a fundamental study of the formation of the PpIX photoproducts, as understanding the formation of photoproducts under various irradiation conditions for PDD and PDT would be useful in dosimetry estimation and may be exploited for improved PDD and PDT.

2 Materials and methods

2.1 Sample irradiation

Protoporphyrin IX (P8293, Sigma-Aldrich, USA) was dissolved in dimethyl sulfoxide (D4540, Sigma-Aldrich) to give a concentration of 10 μM. The PpIX was irradiated to generate the photoproducts using the irradiation setup at the wavelength of 635 nm or 405 nm described in our previous work [22]. For each irradiation wavelength, the photoproduct formation was investigated at irradiation fluence rates of 10 and 100 mW/cm^2. Fluences between 0 and 100 J/cm^2 were used for PpIX irradiation at the wavelength of 635 nm, while 0, 0.6, 1, and 2 J/cm^2 were used for irradiation at the wavelength of 405 nm. To determine the emergence of photoproducts with PpIX irradiation, the absorption spectra, fluorescence spectra, and mass spectra of PpIX before and after irradiation were measured. All analyses, including the sample preparation, were performed in the dark to avoid unexpected photochemical changes in the samples.

Fig. 1 **a** Absorption spectra of PpIX before and after irradiation for 100 J/cm^2 at the wavelength of 635 nm and fluence rates of 10 and 100 mW/cm^2. The absorption spectrum of DMSO was subtracted from that of PpIX. The emergence of a new band at the wavelength of 668 nm was noted after irradiation. **b** Difference spectra of the absorption spectra in **a**. The spectrum of PpIX before irradiation was subtracted from the spectra after irradiation to obtain the difference spectra

2.2 Absorption analysis

The absorbances were measured for PpIX irradiated with a wavelength of 635 nm and fluence of 100 J/cm^2, and wavelength of 405 nm and fluence of 2 J/cm^2. The samples were placed in a quartz cell (F15-UV-10, AS ONE, Japan) having an optical path length of 10 mm, and the absorption spectra for a wavelength range of 400–800 nm were acquired using an ultraviolet–visible spectrophotometer (U-3500, Hitachi, Japan).

2.3 Fluorescence analysis

The fluorescence emissions from the irradiated PpIX were measured for a wavelength range of 550–750 nm using a fluorescence microplate reader (Spectra Max Gemini EM, Molecular Devices, USA) at an excitation wavelength of 405 nm. The obtained fluorescence spectra were corrected for the decreased absorption at the excitation wavelength by normalizing the spectra with the absorbance at 405 nm for each irradiation condition.

2.4 Mass spectrometric analysis

The irradiated samples were further diluted 100-fold with liquid chromatography–mass spectrometry (LC–MS) grade methanol (34,966, Honeywell, Germany) and water (39,253, Honeywell) (v/v 1:1) with 1% acetic acid (00212–85, Nacalai Tesque, Japan), to reduce the concentration of DMSO. The mass spectra were obtained with an electrospray ionization quadrupole time-of-flight mass spectrometer (Q-TOF Ultima API, micromass, UK) in the positive ion mode. The sample was injected at a flow rate of 30 μL/min, and the mass spectra were measured every 0.34 s with a 0.1 s interval and integrated for 3 min.

2.5 High-performance LC (HPLC) analysis

The unirradiated PpIX and irradiated PpIX for 100 J/cm^2 at the wavelength of 635 nm and fluence rate of 10 mW/cm^2 were chromatographically separated using HPLC (Vanquish Flex, Thermo Scientific). The HPLC was performed with an LC column (L-column2 ODS, 3 μm, 2.1 × 50 mm, Metal-free column, Thermo Scientific) maintained at 40 °C with a gradient elution of mobile phases A (distilled water with 0.1% formic acid) and B (acetonitrile with 0.1% formic acid) and a flow rate of 0.3 mL/min. The mobile phase ratio A:B (v/v) was started at 50:50, changed to 5:95 (2–4 min), and back to 50:50 (4–6 min). The output of the HPLC was coupled to an Orbitrap mass spectrometer (Orbitrap Exploris 240, Thermo Scientific), and the separated samples were analyzed in the MS mode and the MS/MS mode at collision energies of 40 and 60 eV.
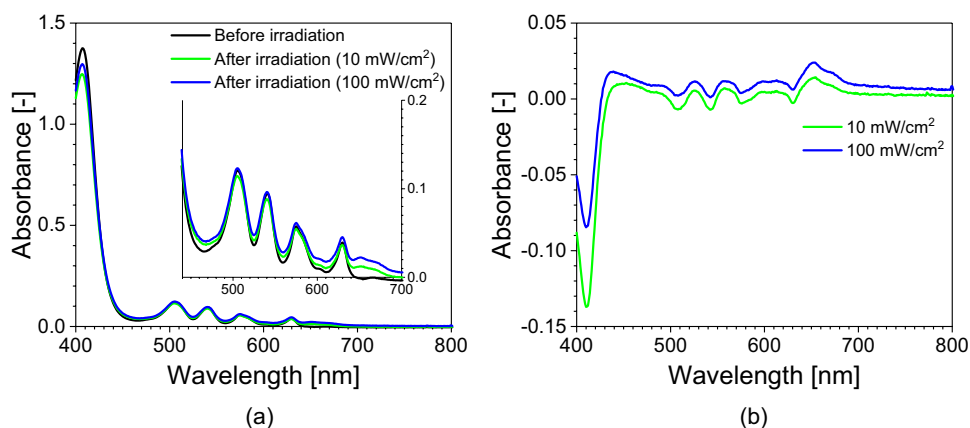
3 Results and discussion

3.1 Absorption analysis of photoproducts

3.1.1 Irradiation at 635 nm

The absorption spectra of PpIX before and after irradiation at the wavelength of 635 nm and fluence rates of 10 and 100 mW/cm^2 are given in Fig. 1a. Prior to irradiation, the absorbance of PpIX at 405 nm was 1.36, while that at 635 nm was 0.02. PpIX irradiation resulted in a decrease in the intensities as well as the broadening of the PpIX peaks in both the Soret and the Q bands. After 100 J/cm^2 irradiation, the absorbance at 405 nm decreased to 0.73 and 0.85, while the absorbance at 635 nm decreased to 0.013 and 0.016 for fluence rates at 10 and 100 mW/cm^2, respectively. The irradiated spectra also exhibited a new absorption band in the wavelength range of 650–670 nm, with a distinct peak at the wavelength of 668 nm. The difference spectra in Fig. 1b were

Fig. 2 a Absorption spectra of PpIX before and after irradiation for 2 J/cm^2 at the wavelength of 405 nm and fluence rates of 10 and 100 mW/cm^2. The absorption spectrum of DMSO was subtracted from that of PpIX. A wide absorption band in the wavelength of 650–700 nm emerges after irradiation. **b** Difference spectra of the absorption spectra in **a**. The spectrum of PpIX before irradiation was subtracted from the spectra after irradiation to obtain the difference spectra

generated by subtracting the spectra of PpIX before irradiation from the irradiated spectrum for each fluence rate. The difference spectra showed an increase in absorbance at the wavelengths of 448, 560, 615, and 668 nm, indicating the formation of photoproducts. The new absorption band at the wavelength of 668 nm (Fig. 1a) is that of the chlorin-type hydroxyaldehyde photoproduct, photoprotoporphyrin (Ppp) [18, 23, 24]. A study has shown a high fluorescence intensity of Ppp when excited at the wavelength of 450 nm [2], indicating that Ppp has one of its absorption bands around 450 nm. Thus, it can be presumed that the absorption peak at the wavelength of 448 nm also belongs to Ppp. The difference spectra (Fig. 1b) show that Ppp formation is favored at lower irradiation fluence, as the intensities of Ppp at the wavelengths of 448 and 668 nm were notably higher for irradiation at 10 mW/cm^2 than at 100 mW/cm^2. The smaller absorption bands detected in the difference spectra indicate the formation of the formyl photoproducts. The absorption bands of the formyl photoproducts of PpIX dimethyl ester

considerably overlap in the wavelength of 430–650 nm with the peaks seen in the present difference spectra [25].

3.1.2 Irradiation at 405 nm

The absorption spectra of PpIX after irradiation at the wavelength of 405 nm for 2 J/cm^2 showed a decrease in the absorbance at 405 nm to 1.24 and 1.28 and a decrease in the absorbance at 635 nm to 0.022 and 0.031 for fluence rates at 10 and 100 mW/cm^2, respectively (Fig. 2a). The absorption spectra of irradiated PpIX indicate the formation of photoproducts by the emergence of a broad absorption peak in the wavelength range of 650–700 nm and the widening of the PpIX peaks. A similar increase in the absorption intensity after PpIX irradiation with the wavelength of 635 nm was observed in the difference spectra after irradiation at the wavelength of 405 nm (Fig. 2b). Thus, it is presumed that both Ppp and the formyl photoproducts are generated after PpIX irradiation at the wavelength of 405 nm. A higher
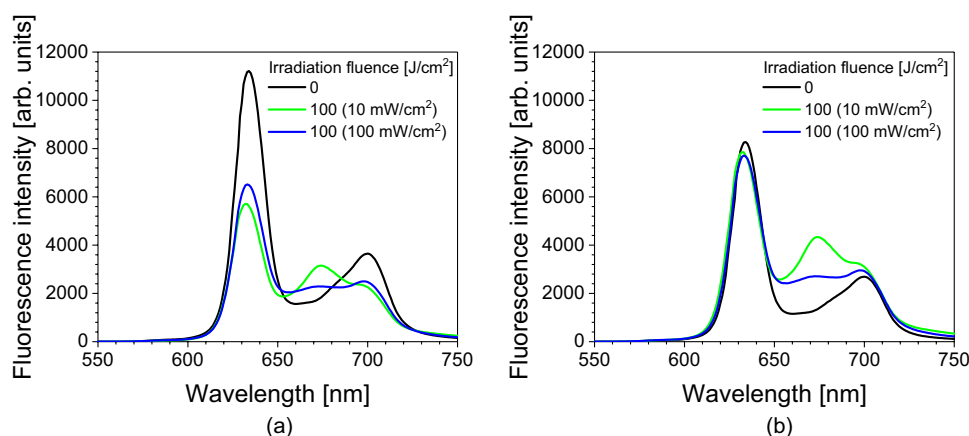
Fig. 3 a Fluorescence spectra of PpIX before and after irradiation with a wavelength of 635 nm for 100 J/cm^2 at fluence rates of 10 and 100 mW/cm^2. The fluorescence were detected at an excitation wavelength of 405 nm. The fluorescence spectrum of DMSO at the same excitation wavelength was subtracted from the PpIX spectra. **b** Fluorescence spectra of **a** corrected for decreased absorbance. The emergence of a new peak at 673 nm was noted in the fluorescence spectra after irradiation
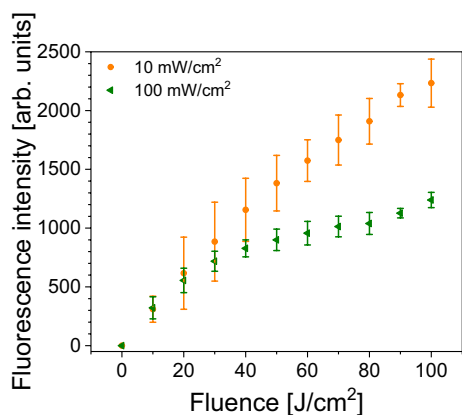
Fig. 4 Fluorescence intensity of PpIX with increasing fluence irradiated at the wavelength of 635 nm and fluence rates of 10 and 100 mW/cm^2. The fluorescence intensity at 673 nm was monitored at an excitation wavelength of 405 nm. The intensities at 673 nm were corrected to exclude the PpIX fluorescence intensities. The error bars indicate the standard deviation from at least 3 independent experiments

absorbance of photoproducts was observed for PpIX irradiation at 100 mW/cm^2 than at 10 mW/cm^2 for PpIX irradiation at the wavelength of 405 nm. The highest absorption peak of the difference spectra occurred at the wavelength of 650 nm, which indicates that the dominant photoproduct is the formyl photoproduct [9, 26].

3.2 Fluorescence analysis of photoproducts

3.2.1 Irradiation at 635 nm

The changes in the fluorescence spectra of PpIX before and after irradiation at the wavelength of 635 nm and fluence rates of 10 and 100 mW/cm^2 are shown in Fig. 3a. The photobleaching of the PpIX peaks at 633 and 700 nm occurred after irradiation. The PpIX photobleaching did not vary considerably between the two fluence rates, as no notable difference between the fluorescence intensities of PpIX after irradiation (100 J/cm^2) between the two fluence rates was seen. After PpIX irradiation, a new fluorescence band appeared at 673 nm. The fluorescence spectra corrected for the decreased absorbance (Fig. 3b) indicate the clear formation of this band. Based on the emission wavelength, the peak at 673 nm is attributed to Ppp [2, 14]. For the PpIX irradiation at the fluence rate of 10 mW/cm^2, the intensity of Ppp was higher compared with irradiation at 100 mW/cm^2.

The formation of Ppp with increasing PpIX irradiation was evaluated by monitoring the fluorescence intensity of the peak at the wavelength of 673 nm for irradiation between 0 and 100 J/cm^2 (Fig. 4). The fluorescence intensity at the wavelength of 673 nm was corrected to exclude the intensity of PpIX by using a correction factor employed elsewhere [2].

The correction factor was obtained by dividing the fluorescence intensity at the wavelength of 673 nm before irradiation (I^0_{673}) with the fluorescence intensity at the wavelength of 633 nm before irradiation (I^0_{633}) and multiplying the ratio by the intensity at the wavelength of 633 nm after irradiation (I'_{633}). The correction factor was then subtracted from the fluorescence intensity at the wavelength of 673 nm after irradiation (I'_{673}):

$$I_{pp673}' = I_{673}' - I_{633}' \times \frac{I^0_{673}}{I^0_{633}}$$

An increase in the intensity of Ppp was observed with increased fluence (Fig. 4). The plot indicates a difference in the rate of Ppp formation with the fluence rate. A higher intensity of Ppp was seen in PpIX irradiated at a lower fluence rate. For irradiation at 10 mW/cm^2, no decrease in the formation of Ppp was seen up to the maximum fluence investigated (100 J/cm^2), and a further increase in the intensity of Ppp can be expected with further irradiation of PpIX at 10 mW/cm^2. On the other hand, Ppp formation began to slow down at approximately 40 J/cm^2 for irradiation at 100 mW/cm^2. The intensity of Ppp was 1.8 times higher for irradiation fluence rate at 10 mW/cm^2 than at 100 mW/cm^2 after 100 J/cm^2.

3.2.2 Irradiation at 405 nm

PpIX irradiation with the wavelength of 405 nm also led to a similar photobleaching rate of the two PpIX peaks between the two fluence rates (Fig. 5a). Irradiation performed at a 10 mW/cm^2 had 74.4% of PpIX left after 2 J/cm^2, and the irradiation at 100 mW/cm^2 had 73.1% PpIX left after similar irradiation fluence. The fluorescence spectra of PpIX after irradiation at the wavelength of 405 nm showed a new peak at the wavelength of 654 nm. This peak was also present in the fluorescence spectra corrected for the decreased absorbance (Fig. 5b). A higher fluorescence intensity of this peak was observed for PpIX irradiation at the fluence rate of 100 mW/cm^2 than at 10 mW/cm^2 (1.2 times intensity at 654 nm for PpIX irradiation at 100 mW/cm^2 than at 10 mW/cm^2 after 2 J/cm^2). The peak at the wavelength of 654 nm is attributed to a photoproduct of PpIX and has been named product II (Pp II) by some authors [5]. Comparing the results with those of absorption analysis (Fig. 2), it may be surmised that this photoproduct is the formyl porphyrin photoproduct, as a similar trend as that observed in the absorption analysis was seen in the fluorescence analysis.

It has been reported that Pp II is primarily a product of Ppp [5]. Thus, the peak of Ppp can be expected in the fluorescence spectra where the peak of Pp II was detected. In the fluorescence spectra of the irradiated PpIX at the wavelength of 405 nm, although the fluorescence peak of Pp II
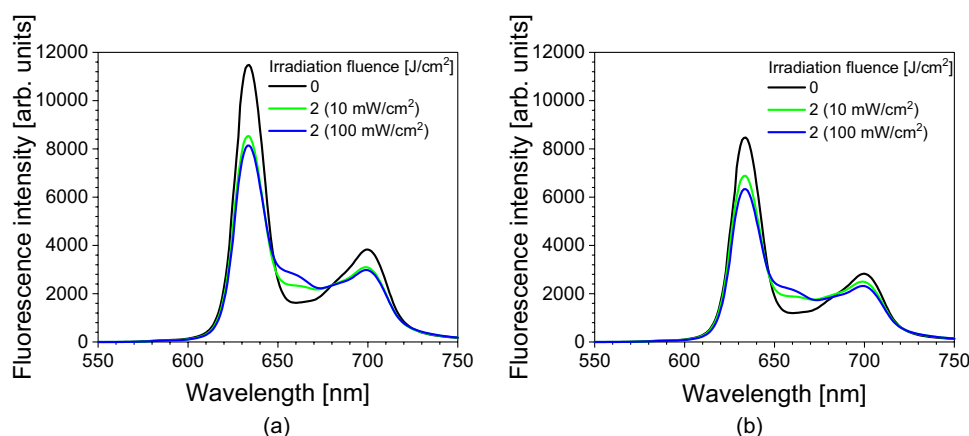
Fig. 5 **a** Fluorescence spectra of PpIX before and after irradiation with a wavelength of 405 nm for 2 J/cm² at fluence rates of 10 and 100 mW/cm². The fluorescence were detected at an excitation wavelength of 405 nm. The fluorescence spectrum of DMSO at the same excitation wavelength was subtracted from the PpIX spectra. **b** Fluorescence spectra of **a** corrected for decreased absorbance. The emergence of a new peak at the wavelength of 654 nm was noted in the fluorescence spectra after irradiation

is present, the peak of Ppp is absent (Fig. 5). In the work by Dysart et al. [5], the fluorescence peaks of both Ppp and Pp II could be observed in the fluorescence spectrum of irradiated PpIX after a detailed spectra decomposition. Considering that the fluorescence peaks of the photoproducts notably overlap with that of PpIX, a similar spectral decomposition as the previous work may be required to detect Ppp and Pp II simultaneously in Fig. 5. If each photoproduct is selectively excited, the fluorescence peak may be detected individually from the same irradiated PpIX [2, 18]. Based on some studies, selective irradiation of Ppp at 670 nm would yield a fluorescence peak around 650 nm (Pp II) when excited at the wavelength of 450 or 543 nm [2, 18]. Others saw a contrasting result on Pp II formation from Ppp in the analysis of the photobleaching of Ppp obtained from PpIX dimethyl ester [17], as no new absorption band in the visible region was detected in the irradiated Ppp. It was proposed that if any photoproducts were formed from the irradiation of Ppp, they may be quickly degraded.

3.3 Mass spectrometric analysis of photoproducts

3.3.1 Irradiation at 635 nm

The mass spectra of the irradiated PpIX at the wavelength of 635 nm (Fig. 6) showed a decrease in the signal intensity of the protonated monoisotopic peak of PpIX at *m/z* 563.3 due to the photobleaching of PpIX. Further, irradiation resulted in the emergence of a peak at *m/z* 595.3. The insets of Fig. 6 show a closer view of the *m/z* where the new peaks were observed. The new peak at *m/z* 595.3 was presumed to belong to a PpIX photoproduct, with the isotope components at *m/z* 596.3 and *m/z* 597.3. For PpIX in solution, oxidation is the main pathway for forming the photoproducts, and

the hydroxyaldehyde photoproduct is formed by the addition of singlet oxygen to either of the PpIX vinyl groups [27, 28]. In line with this, the MS peak at *m/z* 595.3 observed in irradiated PpIX at the wavelength of 635 nm (Fig. 6) is the protonated monoisotopic peak of Ppp. Irradiation of PpIX dimethyl ester at the wavelength of 635 nm under similar conditions as PpIX also showed new MS peaks, which can be explained by the photooxidation of the PpIX dimethyl ester (Fig. S1). Inhoffen et al. [28] analyzed chromatographically separated Ppp formed by the action of light on PpIX dimethyl ester using MS, corroborating that the formation of Ppp is based on the photooxidation of the photosensitizer.

The changes in the signal intensity of the Ppp at *m/z* 595.3 with increased fluence were plotted (Fig. 7). The MS signal intensities were directly compared under the assumption that the signal intensity at *m/z* 595.3 is contributed only by Ppp. Similar to the result of fluorescence analysis, the rise in the intensity of Ppp with irradiation was more dominant for PpIX irradiation at 10 mW/cm² than at 100 mW/cm². The intensity of Ppp after PpIX irradiation for 100 J/cm² was 2.8 times higher for irradiation performed at a fluence rate of 10 mW/cm² than at 100 mW/cm².

3.3.2 PpIX irradiation at 405 nm

The mass spectra of PpIX irradiated at the wavelength of 405 nm showed a noticeable difference in the photobleaching of the protonated monoisotopic peak of PpIX (*m/z* 563.3) between the two fluence rates (Fig. 8). After 1 J/cm² of irradiation at 10 and 100 mW/cm², the intensity of PpIX decreased to 74% and 34%, respectively. This is contrary to what was observed in the fluorescence analysis, where the PpIX photodegration did not differ significantly with the fluence rate. The peak of Ppp at *m/z* 595.3 was absent, and

Fig. 6 Normalized mass spectra of PpIX before and after irradiation for 100 J/cm^2 at the wavelength of 635 nm and fluence rates of **a** 10 and **b** 100 mW/cm^2. The insets show the mass spectra zoomed in around m/z 595.3, where the new peaks were observed
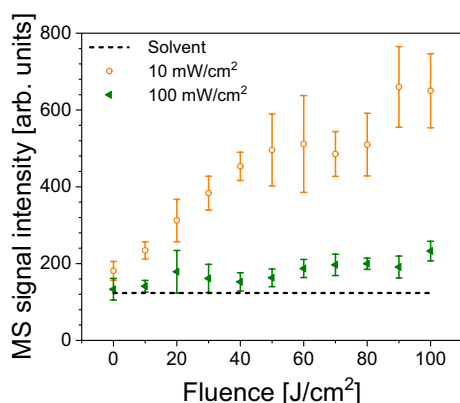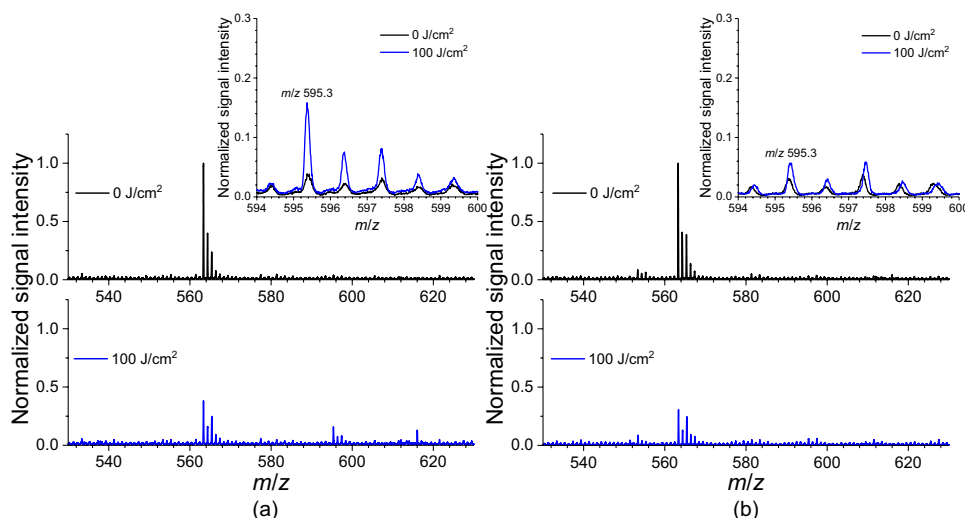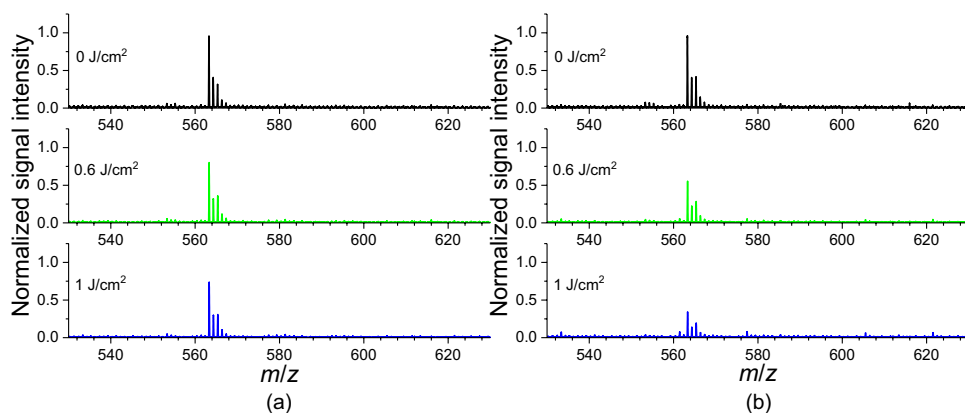

Fig. 7 MS intensity of the protonated monoisotopic peak of Ppp at m/z 595.3 with increased fluence for PpIX irradiation at the wavelength of 635 nm and fluence rates of 10 and 100 mW/cm^2. The error bars indicate the standard deviation from at least 3 independent experiments. The average intensity of the solvent for the m/z analyzed is displayed in a dashed line to indicate the background level

no evident new peak was detected in the mass spectra of PpIX after irradiation at the wavelength of 405 nm (Fig. 8).

The formyl photoproducts have a monoisotopic molecular mass of 564.24 or 566.22 Da [8, 17], and accordingly, the protonated monoisotopic ion of these photoproducts would be detected at m/z 565.24 and 567.22. Although the absorption spectra of irradiated PpIX (Figs. 1 and 2) suggest the formation of the formyl photoproducts, their peaks were not apparent in the mass spectra of the irradiated PpIX (Figs. 6 and 8). The formation rate of the formyl photoproduct is 10 times less than that of Ppp [29], and the MS peaks of the formyl photoproducts overlap with the protonated isotopic peaks of PpIX, possibly hindering their detection. A higher PpIX irradiation, which can increase the formation of the formyl photoproduct, may help in their detection. Additionally, in micelles and liposomes, the dominance of the formyl photoproducts over the hydroxyaldehyde photoproducts has been reported [17]. Thus, investigations of their formation rates in such solvents may be useful.

Fig. 8 Normalized mass spectra of PpIX before and after irradiation for 0.6 and 1 J/cm^2 at the wavelength of 405 nm and fluence rates of **a** 10 and **b** 100 mW/cm^2

3.4 HPLC analysis of photoproducts

Figure 9 shows the extracted ion chromatograms (EIC) of PpIX before and after irradiation at the wavelength of 635 nm for m/z 563.3 (protonated monoisotopic ion of PpIX) and for m/z 595.3 (protonated monoisotopic ion of Ppp). The photobleaching of PpIX after irradiation is indicated by the decreased intensity of the EIC for m/z 563.3 (Fig. 9b). PpIX irradiation also resulted in the formation of three chromatographic peaks (Peaks A, B, and C) for m/z 595.3. The chromatogram peaks suggest the existence of at least three isomers of Ppp. A similar chromatographic separation also occurred in PpIX dimethyl ester irradiated at the wavelength of 635 nm (Fig. S2).

The mass spectra of the LC/MS/MS for the precursor ion at m/z 595.3 for Peaks A, B, and C (Fig. 10) have similar fragmentation patterns, further indicating that these compounds have similar molecular structures. The fragmentation pattern of these peaks is also similar to that of PpIX [30], inferring that these new peaks have a chemical structure similar to that of PpIX. The chemical structures of two isomers of Ppp and their formation mechanisms have been reported previously [28] (Fig. 11). An intermediate is formed by 2,4 cycloaddition of singlet oxygen to the vinyl-substituted diene of PpIX (1→2). The endoperoxide in the intermediate then rearranges to form the hydroxyaldehyde photoproducts (2→3). An analysis of a higher concentration of Ppp may further split the chromatographic peaks at m/z 595.3 observed in the mass spectra for PpIX irradiated at the wavelength of 635 nm (Fig. 9). A third and a fourth isomer may be proposed by the oxygenation of the pyrrolidine ring containing the NH.
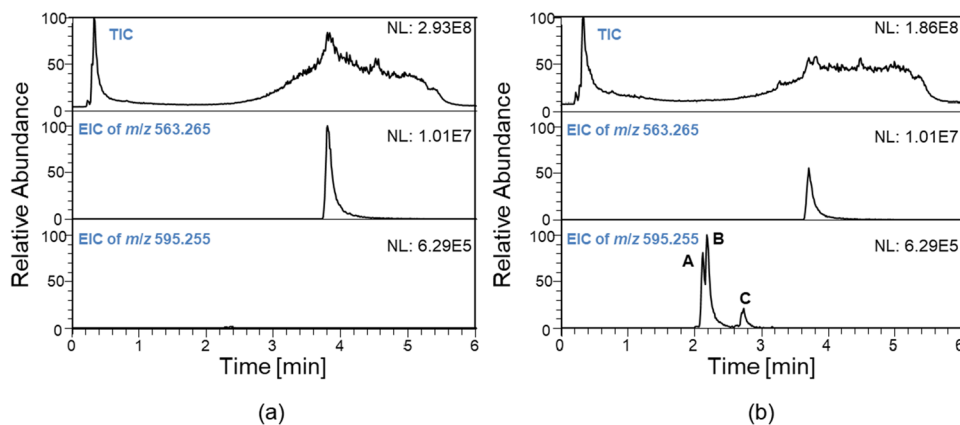
The formyl-type photoproducts are also primarily formed by the reaction of PpIX with singlet oxygen [17, 29, 31]. In their formation, the double bond of PpIX is left intact, and singlet oxygen is directly added to either or both of the vinyl groups to form a dioxetane (1→2). The dioxetane then cleaves to form the formyl photoproduct (2→3) (Fig. 12) [17].

Irradiation of PpIX causes the formation of PpIX photoproducts: hydroxyaldehyde and formyl photoproducts. Both the fluorescence and the absorption peaks of the photoproducts fall in regions similar to that of PpIX. It is surmised that both photoproducts may exist in different quantities after PpIX irradiation. The hydroxyaldehyde photoproduct may be dominant under the red-light irradiation of PpIX, while more formyl photoproducts are formed in the blue-light irradiation of PpIX. In addition, the dependence of the photoproduct formation with the irradiation fluence rate was noted. A higher formation of the photoproduct at a low fluence rate for PpIX irradiated at the wavelength of 635 nm was observed (Figs. 1, 3, and 6). On the contrary, PpIX irradiation with the wavelength of 405 nm indicated a higher photoproduct formation at a higher fluence rate (Figs. 2 and 5). Differences in the irradiation time and energy between the irradiation wavelengths may result in differences in the reaction rates for the photoproduct formation. A fast reaction rate may occur for irradiation with 405 nm, where PpIX has the highest absorption. Any Ppp that may have formed may be quickly oxidized to form another compound. Further, the amount of singlet oxygen necessary for the photoproduct formation is generated at different rates at different irradiation wavelengths [32, 33], and differences in the amount of photoproduct formed with the irradiation wavelength may arise. Oxygen concentration may also play a role. The effect of fluence rate on oxygen availability has been previously reported by some authors [12, 34, 35], and can affect the singlet oxygen production. However, some have reported a contrary result, as no oxygen dependence on the fluence rate was noted in the treatment region [36, 37].

The prospect of applying PpIX photoproducts for extended fluorescence diagnosis and laser therapy has already been highlighted [14, 16, 20, 26, 38]. The photoproducts have similar or less susceptibility to photobleaching as PpIX [2, 10, 27, 39]. Under PDT irradiation condition at

Fig. 9 Total ion chromatogram (TIC) and extracted ion chromatogram (EIC) of PpIX **a** before and **b** after irradiation at the fluence of 100 J/cm². PpIX was irradiated at the wavelength of 635 nm and fluence rate of 10 mW/cm². The TIC and the EIC were obtained at m/z 563.3 and m/z 595.3. NL: Normalization Level
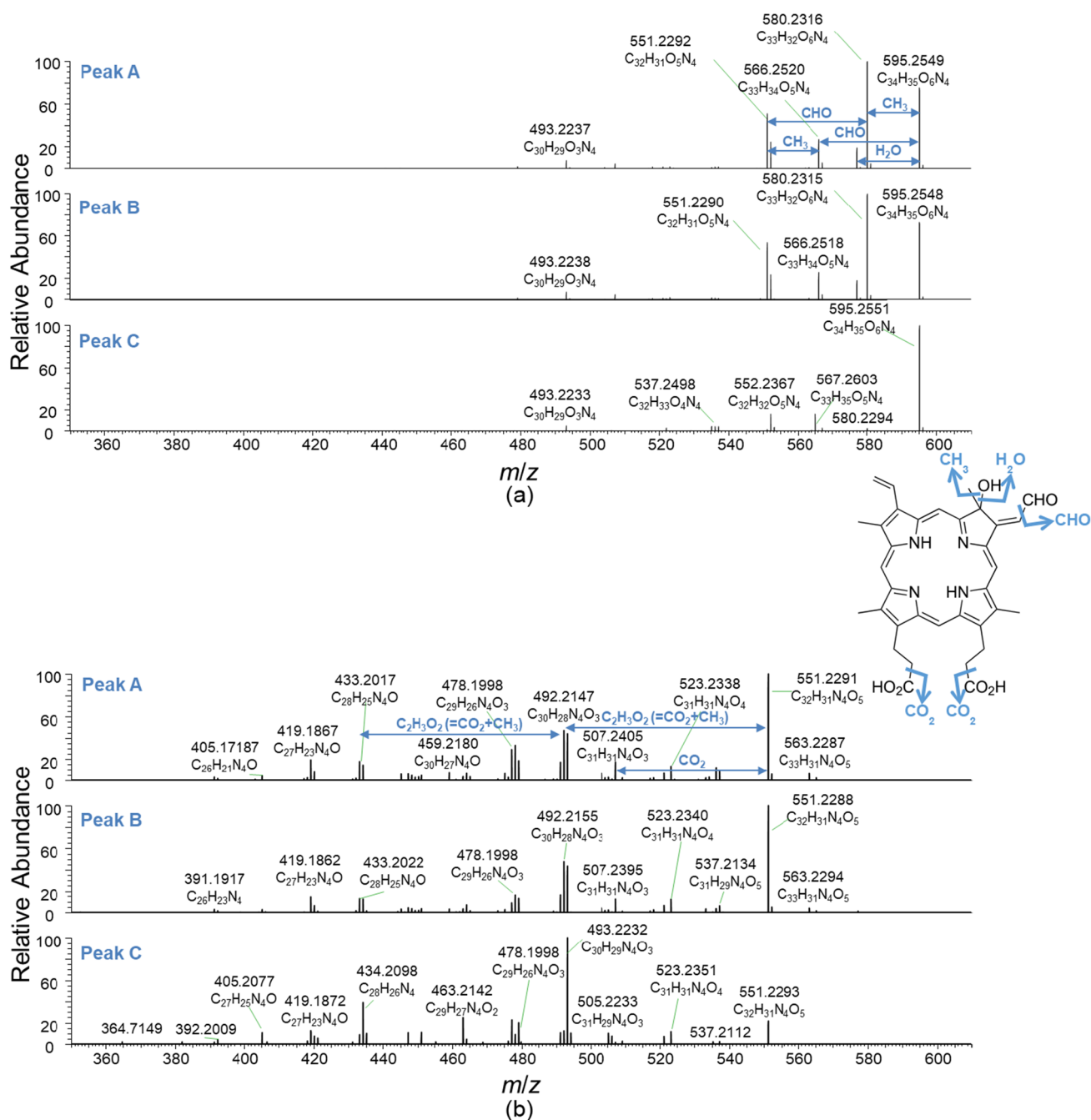
Fig. 10 LC/MS/MS spectra of the peaks A–C in the EIC for *m/z* 595.3 at the collision energy of **a** 40 eV, and **b** 60 eV. The fragmented molecules from the precursor ion at *m/z* 595.3 are displayed on the chemical structure of one of the isomers of the hydroxyaldehyde photoproducts

a low fluence rate, increased photoproduct formation was seen. PDT at a low fluence rate yields higher tumor destruction [36], making PDT at low fluence advantageous. The photoproduct's intensity continued to rise up to the maximum irradiation fluence investigated, implying that extending the irradiation period may benefit PDT. Since a considerable amount of photoproducts are formed under such excitation, the photoproducts could be instrumental to PDT if explored. In some fluorescence diagnoses, higher fluence rates are desired [40–43]. Irradiation with 405 nm, typically used in PDD, yields higher photoproducts for high fluence rates. In such cases, the excitation of the photoproduct could be used in addition to PpIX excitation for extended tumor detection [20]. However, the irradiation conditions for PDD and PDT need to be adjusted accordingly for the desired photoproduct formation.
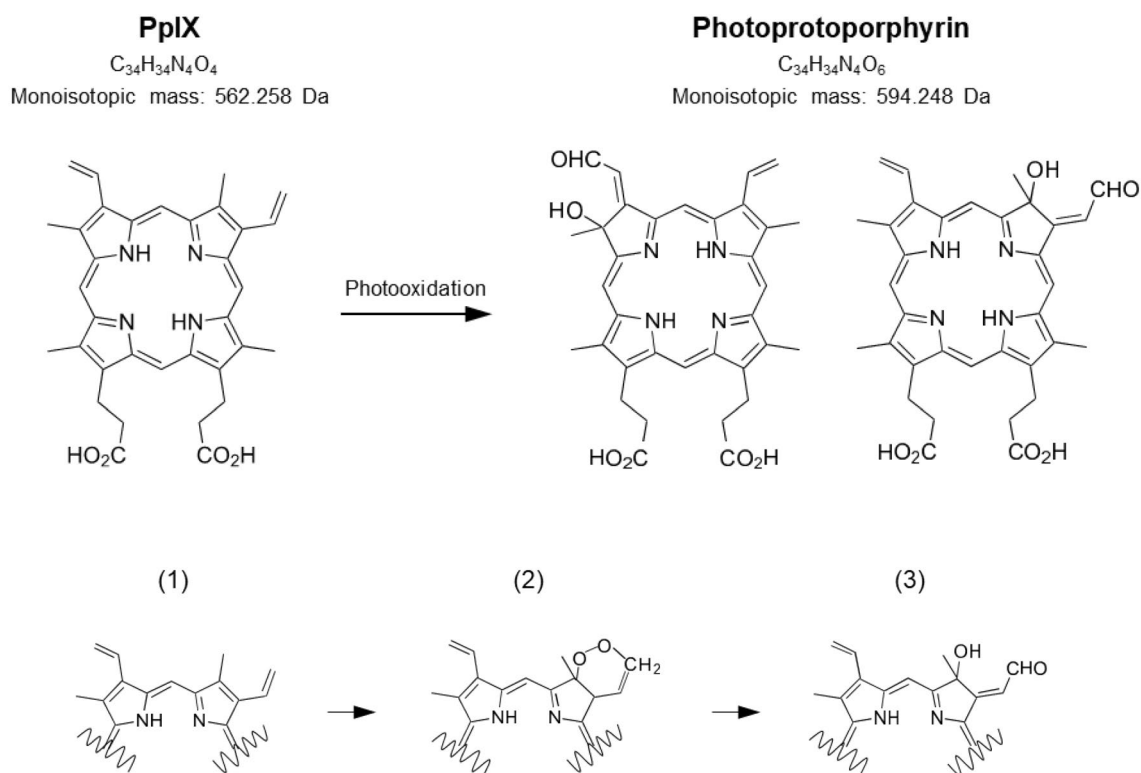
Fig. 11 Chemical structure of the isomers of hydroxyaldehyde photoproduct, photoprotoporphyrin, and their reaction scheme. $1 \rightarrow 2$: 2,4 cycloaddition of singlet oxygen to the vinyl-substituted diene of PpIX to form an intermediate. $2 \rightarrow 3$: The endoperoxide in the intermediate then rearranges to form the hydroxyaldehyde photoproducts [28]

The photoproducts observed in the present study have also been observed in different cells and in vivo analysis [2, 5, 6, 8, 11, 12, 38]. The results of the present analyses indicate that the photoproduct formation is dependent on the irradiation light. The formation of photoproducts also depends on environmental factors, which vary with the biological system [2, 5]. Analysis comparing the photoproduct formation from PpIX and its dimethyl ester in cells and organic solvents reported different formation distributions of the photoproducts with the PpIX environment [8–10, 38]. Thus, investigation of the detailed formation of these photoproducts in vivo is necessary if their utilization is intended in PDD and PDT.

4 Conclusion

The results obtained in this study show that the dominant PpIX photoproduct formed differs with the PpIX irradiation wavelength. Additionally, the photoproduct formation rate varies with the fluence rate. Photooxidation is the main pathway for the formation of these photoproducts. The disparity in the singlet oxygen production with the wavelength used in the PpIX irradiation and the fluence rate can lead to variations in the reaction rates for the photoproduct formations. Analyses in this study were performed with PpIX in DMSO, and the results may vary when performed in a biological environment. However, the results obtained in the present work serve as a foundation and would be instrumental for future analysis of photoproduct formation in more complex in vivo environments.
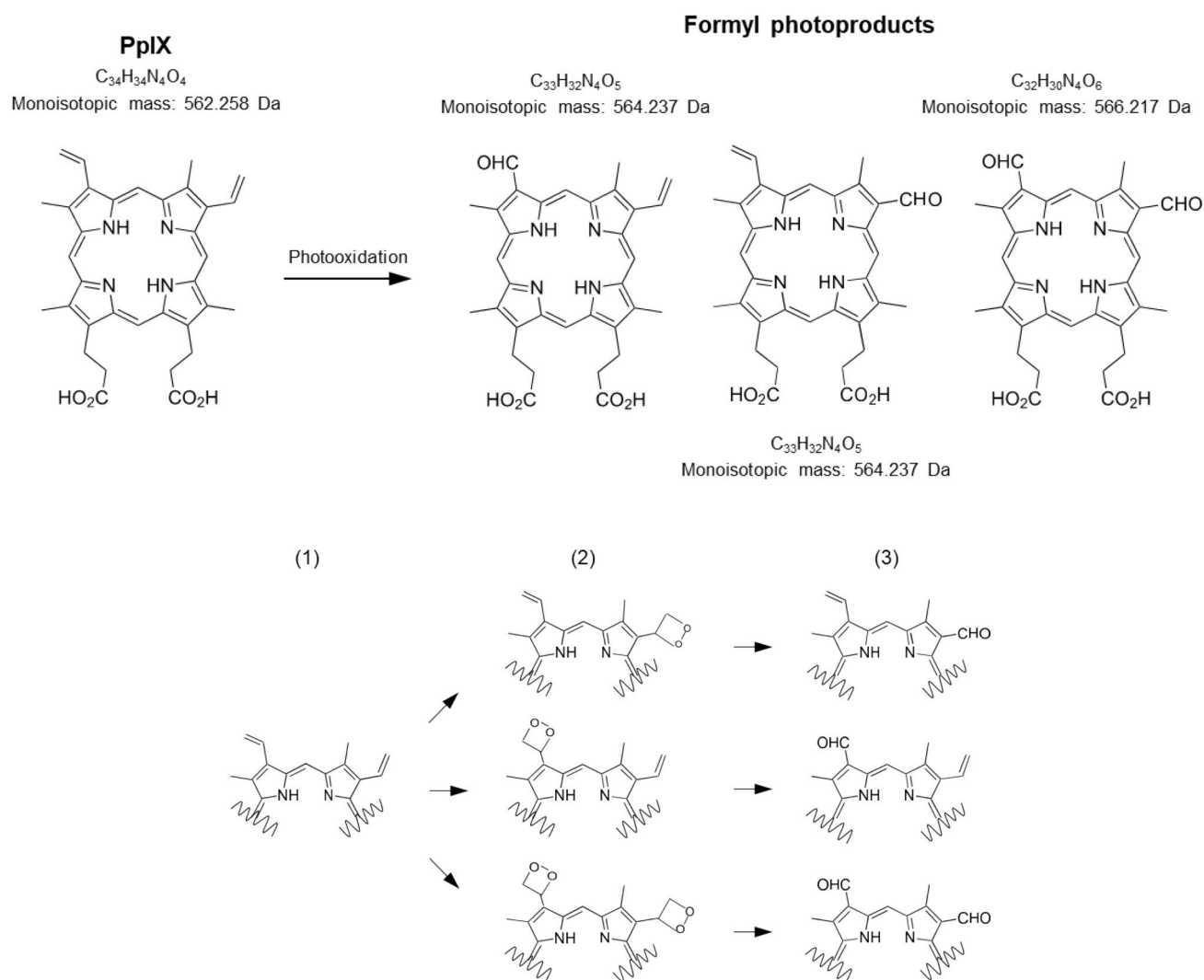
Fig. 12 Chemical structure of the isomers of formly photoproducts and their reaction scheme. $1 \rightarrow 2$: Singlet oxygen is directly added to either or both of the vinyl groups to form a dioxetane. $2 \rightarrow 3$: The dioxetane cleavages to form the formyl photoproduct [17]

Data availability Not applicable.

Declarations

Conflict of interest The authors have no competing interests to declare.

References

1. Li, X., Zhao, C., Kou, H., Zhu, F., Yang, Y., & Lu, Y. (2022). PDD-guided tumor excision combined with photodynamic therapy in patients with extramammary Paget's disease. *Photodiagnosis and Photodynamic Therapy, 38*, 102841.

2. Bagdonas, S., Ma, L. W., Iani, V., Rotomskis, R., Juzenas, P., & Moan, J. (2000). Phototransformations of 5-aminolevulinic acid–induced Protoporphyrin IX in vitro: a spectroscopic study. *Photochemistry and Photobiology, 72*(2), 186–192.

3. Teng, K. W., & Lee, S. H. (2019). Characterization of protoporphyrin IX species in vitro using fluorescence spectroscopy and polar plot analysis. *Journal of Physical Chemistry B, 123*(27), 5832–5840.

4. Bown, S. G., & Stepp, H. (2015). Photodynamic diagnosis and therapy - How bright is the future? *Photonics and Lasers in Medicine, 4*(1), 1–3.

5. Dysart, J. S., & Patterson, M. S. (2006). Photobleaching kinetics, photoproduct formation, and dose estimation during ALA induced PpIX PDT of MLL cells under well oxygenated and hypoxic conditions. *Photochemical and Photobiological Sciences, 5*(1), 73–81.

6. Huang, K., Chen, L., Lv, S., & Xiong, J. (2012). Protoporphyrin IX photobleaching of subcellular distributed sites of leukemic HL60 cells based on ALA-PDT in vitro. *Journal of Biomedical Science and Engineering, 05*(09), 548–555.

7. Efendiev, K., Alekseeva, P., Shiryaev, A., Voitova, A., Linkov, K., Pisareva, T., Reshetov, I., & Loschenov, V. (2023). Near-infrared phototheranostics of tumors with protoporphyrin IX and chlorin e6 photosensitizers. *Photodiagnosis and Photodynamic Therapy, 42*, 103566.

8. Wessels, J. M., Sroka, R., Heil, P., & Seidlitz, H. K. (1993). Photodegradation of protoporphyrin-dimethylester in solution and in organized environments. *International Journal of Radiation Biology, 64*(5), 475–484.

9. Horsey, B. E., & Whitten, D. G. (1978). Photochemical reactions in organized monolayer assemblies. 8. environmental effects on photochemical reactions: contrasts in the photooxidation behavior of protoporphyrin IX in solution, monolayer films, organized monolayer assemblies, and micelles. *Journal of the American Chemical Society, 100*(4), 1293–1295.

10. Dietel, W., & Wendenburg, R. (1995). Phototransformation of ALA-induced protoporphyrin IX (PPIX) in carcinoma cells and of exogenous PPIX in cells and solutions. *SPIE, 2371*, 567–571.

11. Af Klinteberg, C., Enejder, A. M. K., Wang, I., Andersson-Engels, S., Svanberg, S., & Svanberg, K. (1999). Kinetic fluorescence studies of 5-aminolaevulinic acid-induced protoporphyrin IX accumulation in basal cell carcinomas. *Journal of Photochemistry and Photobiology B: Biology, 49*(2–3), 120–128.

12. Finlay, J. C., Conover, D. L., Hull, E. L., & Foster, T. H. (2001). Porphyrin bleaching and PDT-induced spectral changes are irradiance dependent in ALA-sensitized normal rat skin in vivo. *Photochemistry and Photobiology, 73*(1), 54–63.

13. Brancaleon, L., & Moseley, H. (2002). Effects of photoproducts on the binding properties of protoporphyrin IX to proteins. *Biophysical Chemistry, 96*(1), 77–87.

14. Ma, L., Bagdonas, S., & Moan, J. (2001). The photosensitizing effect of the photoproduct of protoporphyrin IX. *Journal of Photochemistry and Photobiology B: Biology, 60*(2–3), 108–113.

15. Moan, J., Streckyte, G., Bagdonas, S., Bech, Ø., & Berg, K. (1997). Photobleaching of protoporphyrin IX in cells incubated with 5-aminolevulinic acid. *International Journal of Cancer, 70*, 90–97.

16. Giniūnas, L., Rotomskis, R., Smilgevičius, V., Piskarskas, A., Didžiapetrienė, J., Bloznelyte, L., & Griciute, L. (1991). Activity of haematoporphyrin derivative photoproduct in photodynamic therapy in vivo. *Lasers in Medical Science, 6*(4), 425–428.

17. Cox, G. S., & Whitten, D. G. (1983). Excited state interactions of protoporphyrin IX and related porphyrins with molecular oxygen in solutions and in organized assemblies. *Advances in experimental medicine and biology, 160*, 279–292.

18. Theodossiou, T., & MacRobert, A. J. (2002). Comparison of the photodynamic effect of exogenous photoprotoporphyrin and protoporphyrin IX on PAM 212 murine keratinocytes. *Photochemistry and Photobiology, 76*(5), 530–537.

19. Kubát, P., Zelinger, Z., & Jirsa, M. (1997). The effect of the irradiation wavelength on the processes sensitized by protoporphyrin IX dimethyl ester. *Radiation Research, 148*(4), 382–385.

20. Ogbonna, S. J., York, W. Y., Nishimura, T., Hazama, H., Fukuhara, H., Inoue, K., & Awazu, K. (2023). Increased fluorescence observation intensity during the photodynamic diagnosis of deeply located tumors by fluorescence photoswitching of protoporphyrin IX. *Journal of Biomedical Optics, 28*(5), 055001.

21. Rossetti, F. C., Depieri, L. V., Tedesco, A. C., & Bentley, M. V. L. B. (2010). Fluorometric quantification of protoporphyrin IX in biological skin samples from in vitro penetration/permeation studies. *Brazilian Journal of Pharmaceutical Sciences, 46*(4), 753–760.

22. Ogbonna, S. J., Hazama, H., & Awazu, K. (2021). Mass spectrometric analysis of the photobleaching of protoporphyrin IX used in photodynamic diagnosis and therapy of cancer. *Photochemistry and Photobiology, 97*(5), 1089–1096.

23. Charlesworth, P., & Truscott, T. G. (1993). The use of 5-aminolevulinic acid (ALA) in photodynamic therapy (PDT). *Journal of Photochemistry and Photobiology B: Biology, 18*(1), 99–100.

24. Ayala, E. T. P., de Sousa, F. A. D., Vollet-Filho, J. D., Garcia, M. R., De Boni, L., Bagnato, V. S., & Pratavieira, S. (2021). Photodynamic and sonodynamic therapy with protoporphyrin IX in vitro and in vivo studies. *Ultrasound in Medicine Biology, 47*(4), 1032–1044.

25. Wijesekera, T. P., & Dolphin, D. (1985). Some preparations and properties of porphyrins. *Advances in experimental medicine and biology, 193*, 229–266.

26. Dickson, E. F. G., & Pottier, R. H. (1995). On the role of protoporphyrin IX photoproducts in photodynamic therapy. *Journal of Photochemistry and Photobiology, B: Biology, 29*(1), 91–93.

27. Cox, G. S., & Whitten, D. G. (1982). Mechanisms for the photooxidation of protoporphyrin IX in solution. *Journal of the American Chemical Society, 104*(2), 516–521.

28. Inhoffen, H. H., Brockmann, H. Jr., & Bliesener, K. M. (1969). Zur weiteren Kenntnis des Chlorophylls und des Hämins XXX1) Photoprotoporphyrine und ihre Umwandlung in Spirographissowie Isospirographis-porphyrin2). *Justus Liebigs Annalen der Chemie, 730*(1), 173–185.

29. Bonnett, R., & Martínez, G. (2001). Photobleaching of sensitisers used in photodynamic therapy. *Tetrahedron, 57*(47), 9513–9547.

30. Walke, A., Molina, E. S., Stummer, W., & König, S. (2020). Protoporphyrin IX analysis from blood and serum in the context of neurosurgery of glioblastoma. In G. Mitulović (Ed.), *Mass spectrometry in life sciences and clinical laboratory* (pp. 1–17). IntechOpen.

31. Dickson, E. F. G., & Pottier, R. H. (1995). "On the role of protoporphyrin IX photoproducts in photodynamic therapy. *Journal of Photochemistry and Photobiology B Biology, 29*(1), 91–93.

32. Nishimura, T., Hara, K., Honda, N., Okazaki, S., Hazama, H., & Awazu, K. (2020). Determination and analysis of singlet oxygen quantum yields of talaporfin sodium, protoporphyrin IX, and lipidated protoporphyrin IX using near-infrared luminescence spectroscopy. *Lasers in Medical Science, 35*(6), 1289–1297.

33. Jarvi, M. T., Niedre, M. J., Patterson, M. S., & Wilson, B. C. (2006). Singlet Oxygen Luminescence dosimetry (SOLD) for photodynamic therapy: current status, challenges and future prospects. *Photochemistry and Photobiology, 82*(5), 1198.

34. Sudworth, C. D., Stringer, M. R., Cruse-Sawyer, J. E., & Brown, S. B. (2003). Fluorescence microspectroscopy technique for the

study of intracellular protoporphyrin IX dynamics. *Applied Spectroscopy, 57*(6), 682–688.

35. Robinson, D. J., De Bruijn, H. S., Van Der Veen, N., Stringer, M. R., Brown, S. B., & Star, W. M. (1998). Fluorescence photobleaching of ALA-induced protoporphyrin IX during photodynamic therapy of normal hairless mouse skin: the effect of light dose and irradiance and the resulting biological effect. *Photochemistry and Photobiology, 67*(1), 140–149.

36. Iinuma, S., Schomacker, K., Wagnières, G., Rajadhyaksha, M., Bamberg, M., Momma, T., & Hasan, T. (2000). In vivo fluence rate and fractionation effects on tumor response and photobleaching: Photodynamic therapy with two photosensitizers in an orthotopic rat tumor model. *Cancer Research, 59*, 6164–6170.

37. Sørensen, R., Iani, V., & Moan, J. (1998). Kinetics of Photobleaching of Protoporphyrin IX in the Skin of Nude Mice Exposed to Different Fluence Rates of Red Light. *Photochemistry and Photobiology, 68*(6), 835–840.

38. König, K., Schneckenburger, H., Rück, A., & Steiner, R. (1993). In vivo photoproduct formation during PDT with ALA-induced endogenous porphyrins. *Journal of Photochemistry and Photobiology, B: Biology, 18*(2–3), 287–290.

39. Seidlitz, H. K., Stettmaier, K., Wessels, J. M., & Schneckenburger, H. (1992). Intracellular fluorescence polarization, picosecond kinetics, and light-induced reactions of photosensitizing porphyrins. *Optical Engineering, 31*(7), 1482–1486.

40. Buzalewicz, I., Hołowacz, I., Ulatowska-Jarża, A., & Podbielska, H. (2017). Towards dosimetry for photodynamic diagnosis with the low-level dose of photosensitizer. *Journal of Photochemistry and Photobiology B: Biology, 173*, 333–343.

41. Hirano, T., Hagiya, Y., Fukuhara, H., Inoue, K., Shuin, T., Matsumoto, K., Inoue, K., Tanaka, T., Okura, I., & Ogura, S. I. (2013). Improvement of aminolevulinic acid (ALA)-mediated photodynamic diagnosis using n-propyl gallate. *Photodiagnosis and Photodynamic Therapy, 10*(1), 28–32.

42. Kurakina, D., Khilov, A., Shakhova, M., Orlinskaya, N., Sergeeva, E., Meller, A., Turchin, I., & Kirillin, M. (2019). Comparative analysis of single- and dual-wavelength photodynamic therapy regimes with chlorin-based photosensitizers: Animal study. *Journal of Biomedical Optics, 25*(06), 1.

43. Namikawa, T., Yatabe, T., Inoue, K., Shuin, T., & Hanazaki, K. (2015). Clinical applications of 5-aminolevulinic acid-mediated fluorescence for gastric cancer. *World Journal of Gastroenterology, 21*(29), 8817–8825.

Authors and Affiliations

Sochi J. Ogbonna[1] · **Katsuyoshi Masuda**[1,2] · **Hisanao Hazama**[1]

✉ Sochi J. Ogbonna
ogbonna-s@mb.see.eng.osaka-u.ac.jp

Hisanao Hazama
hazama-h@see.eng.osaka-u.ac.jp

[1] Division of Sustainable Energy and Environmental Engineering, Graduate School of Engineering, Osaka University, Osaka, Japan

[2] Graduate Course of Human Health Science, Graduate School of Medicine, Kyoto University, Kyoto, Japan